ELSEVIER

Available online at www.sciencedirect.com

SciVerse ScienceDirect

Energy Procedia 20 (2012) 116 – 133

Energy Procedia

Technoport RERC 2012

Prediction of Wave Loads on Tidal Turbine Blades

Céline Faudot[a], Ole Gunnar Dahlhaug[a]

[a] *NTNU, Hydropower laboratory, Alfred Getz vei 4, 7491 Trondheim, Norway*

Abstract

Wave loads are one of the main contributors to fatigue loads of tidal turbine blades. Because of this, they are a determinant parameter for calculation of turbine blade life time. To avoid cost associated with oversizing blades or replacing a damaged blade, it is essential to evaluate the loads acting on the turbine, and especially wave loads on the blades, with the best possible accuracy.

Experience from wind industry is valuable for horizontal axis tidal turbine design and loads acting on the blade can be estimated using the same methods, even if the loads are different. This article presents the main features of a code written with Matlab, able to predict thrust force and torque on each blade while the turbine is operating in a regular wave field. The quasi-static Blade Element Momentum theory is combined here with an added mass force modeling. The linear wave theory is employed to describe the water particle velocity due to waves. This velocity is, as a first approximation, simply added to a uniform stream velocity to account for wave-current interaction.

The analytical results are validated by comparing them with experimental data obtained by testing a 1.475m-diameter rotor towed in a 260m-long wave tank, for different combinations of current speeds and wave characteristics. This emphasizes the importance of wave effects and dynamics in the design of tidal turbine blades.

Keywords: tidal turbine blade; wave loads; blade element momentum theory; dynamic wake

1. Introduction

Tidal turbine rotors are designed following the examples of wind turbine rotors. The environment of both turbines is however very different, in term of density, viscosity, and flow perturbations. The need of models that could predict the blade loads for turbines subjected to such flow is significant, now that the first prototypes are installed offshore. This publication focuses on wave loads and investigates the relevance of including the added mass of the blades in a Blade Element Momentum theory algorithm (BEM), for different sea states. The turbine used as case study is the reference tidal turbine developed at

 doi:10.1016/j.egypro.2012.03.014

NTNU (Trondheim, Norway) and described in Faudot et al. [1]. A model scaled of the rotor of diameter 1.475m and tip speed ratio 7 has been tested in a towing tank and the results in regular wave fields are compared with theoretical results.

2. Background

Masters et al. [2] validated the use of the BEM in uniform flow by comparing it with commercial codes and a lifting line theory method. Concerning tip loss, the commonly used Prandlt's formulation is not very accurate for 2-bladed turbines with high tip speed ratio. Moreover, an inconsistency in the physical meaning of the formulation has been highlighted by Shen et al. It concerns the flow at the tip where the relative axial velocity tends to zero even with non-zero axial flow. That is why the formulation given by Shen et al. (explained further) also adapted for hub loss is chosen. The combination of both losses and BEM being validated by Masters et Al, this method will be used in this paper.

Baltrop et al. [3] investigated the ability of BEM to predict bending moments at the roots of the blades by comparing the results with experiments carried out on a 350mm diameter rotor. A difference between long and steep waves is noticed. The latter involving non-linear effects, the steady BEM in its most simple formulation is not able to give an exact determination of the loads.

The effect of axial inertia and added mass has been experimentally and analytically investigated by Whelan et al. [4] on both an actuator disc and a rotor mounted on a towing carriage and having in addition oscillatory motions. It is shown that the added-mass coefficient of the rotor is small and not obviously dependent on neither the Keulagan Carpenter number nor the tip speed ratio. Which means that even in full scale the added mass will not significantly vary with the wave characteristics, the added mass of the rotor can be assumed as constant. However, the vertical component of wave particle velocity and the depth dependency of the horizontal component are not considered in Whelan's study.

By implementing an added mass model, which will be further explained, in AeroDyn code combined with FAST, Maniaci and Li [5] highlighted the importance of added mass consideration when calculating blade structural loads, i.e. thrust force. Step pitch change cases are studied and, once again, only the axial added mass is considered. In the case of pitch change, the blade itself is moving through the fluid with non-zero acceleration, which may be different from a blade rotating at constant rotational speed in an accelerating fluid. That can explain the difference between Whelan's and Maniaci's conclusions.

The idea here is to adapt the BEM so that it is not applied to an actuator disc or even a rotor but to one blade. As the wave crest passes the swept area, both blades are indeed subjected to different incident velocities due to the exponential shape of wave velocity profiles. It is thus not relevant anymore to look for the loads on the full rotor if the objective is to give a suitable structural design of each blade.

Nomenclature

a	Axial induction factor	-
a'	Rotational induction factor	-
C_D	Drag coefficient	-
C_L	Lift coefficient	-
Cp	Power coefficient	-
F	Tip loss	-
F_D	Drag force	N
F_L	Lift force	N
g	Acceleration of gravity	m/s^2

T_W	Wave period	s
U	Tangential velocity	m/s
V	Current velocity	m/s
V_H	wave particle velocity in horizontal direction	m/s
V_V	wave particle velocity in horizontal direction	m/s
W	Relative velocity	m/s
z	Local water depth	m
Z	Number of blades	-
α	Angle of attack	rd

H_W	Wave height	m
k	Wave number	rd/m
L_C	Chord length	m
Q	Shaft torque	Nm
r	Local radius	m
R	Rotor radius	m
T	Thrust force	N
TSR	Tip Speed Ratio	-

γ	Angular position of blade	rd
φ	Flow angle	rd
μ	Relative current number	-
ρ	Water density	kg/m^3
σ	Local solidity ratio	-
ω	Rotor rotational speed	rd/s
ω_e	Wave rotational frequency of encounter	rd/s
ω_w	Wave rotational frequency	rd/s

3. Blade Element Momentum Theory and added mass

3.1. Steady Blade Element Momentum Theory algorithm in wave field

The Blade Element Momentum Theory (BEM), is a method which can estimate the loads on an horizontal axis wind or tidal turbine, by combining the blade element method and the momentum theory. The reader is referred to Hansen [6] for a detailed description of the method. Batten et al. [7] showed that the loads obtained with this method agree pretty well with experimental methods in uniform flow.

The basis of the code used here is explained in Faudot et al. [1]. The blades are divided into elements and each elementary load, i.e. thrust force and torque, is determined using the hydrodynamic properties of the local hydrofoil. Fig 1 shows one section and the relative velocity vector, W. This relative velocity is the sum of the axial velocity, V_a corrected by the axial induction factor, a and the tangential velocity, V_{rot} obtained from the rotational velocity of the blade and the rotational induction factor, a', as expressed in equations (1) and (2):

$$V_a = (V + V_H) \cdot (1 - a) \tag{1}$$

$$V_{rot} = (\omega \cdot r + V_V \cdot \cos\gamma) \cdot (1 + a') \tag{2}$$

where V is the current velocity, V_H and V_V, are respectively the horizontal and the vertical component of wave particle velocity calculated at the local depth of the blade element, ω is the rotational speed of the blade, and γ is the angular position of the blade, positive counter-clockwise from the current direction.

In the actuator disc theory, a and a' refer to the induction factors of the whole rotor, while here they concern each element separately and are changing in time while waves are passing the swept area. The main objective of the BEM is to determine the values of a and a' by using an iterative approach.

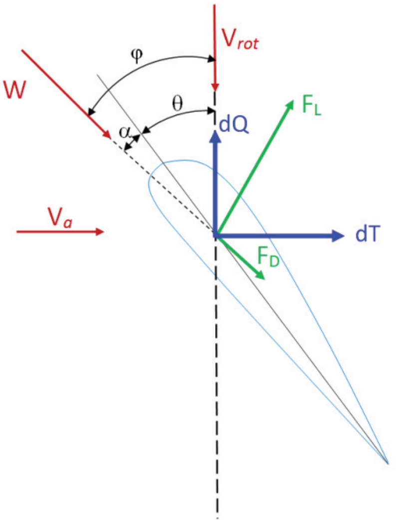

Fig. 1. Velocities and angles on a 2D section

First, initial values of the induction factors are chosen, for example equal to those obtained during the design phase of the blade in uniform inflow. Assuming those induction factors, the relative velocity W encountered by each section can be calculated, as well as the angle of attack so that hydrodynamic coefficients, C_L and C_D are known. A new value of a and a' can then be calculated using the equations (3) and (4).

$$a_{new} = a + \frac{1}{4 \cdot F \cdot \frac{\sin(\varphi)^2}{\sigma \cdot c_a} + 1} \quad (3)$$

$$a'_{new} = a' + \frac{1}{4 \cdot F \cdot \frac{\sin(\varphi) \cdot \cos(\varphi)}{\sigma \cdot c_r} - 1} \quad (4)$$

where F is the tip and hub losses (explained further), φ is the flow angle, σ is the local solidity ratio defined as:

$$\sigma = \frac{Z \cdot L_c}{2 \cdot \pi \cdot r} \quad (5)$$

c_a and c_r are the axial and rotational coefficients defined using lift and drag coefficients as in equations (6) and (7).

$$c_a = C_L \cdot \cos(\varphi) + C_D \cdot \sin(\varphi) \tag{6}$$

$$c_r = C_L \cdot \sin(\varphi) - C_D \cdot \cos(\varphi) \tag{7}$$

If the difference between a_{new} and a, respectively between a'_{new} and a', meets the convergence criterion, the last values of a_{new} and a'_{new} are kept in the following of the method and corrected using Glauert's correction.

Lift and drag coefficients are assumed to be equal to the 2D values obtained with Xfoil [8] at the section where the hydrofoils are standard. To avoid inconsistencies generated by low Reynolds Numbers, Xfoil has been used with model scale Reynolds numbers, but with an equivalent boundary layer turbulent transition point. The transition is indeed forced at the same relative chord length as it would occur on a full-scale 20m-diameter rotor under a 2.5m/s-velocity stream. Those coefficients are linearly interpolated between the sections where the hydrofoils are standard (S816, S825 and S826) as described in [1], so that each element has its own lift and drag coefficients.

Concerning the 3D effects at the tip and the root of the blades, it is common to use Prandlt's tip loss factor. However, Masters et Al [2] compared it with a more recent correction proposed by Shen et al., exposed in equation (8). The latter gives a more realistic distribution of the loads along the blade and the loads agree better with the experiments; therefore it will be used in this study.

$$F_{tip} = \frac{2}{\pi} cos^{-1} \left[exp\left(-b \cdot \frac{Z \cdot (R-r)}{2 \cdot R \cdot \sin(\varphi)} \right) \right] \tag{8}$$

where

$$b = exp[-0.125 \cdot (Z \cdot TSr - 21)]$$

where r is the element radius, R the rotor radius and *TSr* the local speed ratio.
Using the same approach, the hub loss factor is as in equation (9):

$$F_{hub} = \frac{2}{\pi} cos^{-1} \left[exp\left(-b \cdot \frac{Z \cdot (r-R_{Hub})}{2 \cdot R_{Hub} \cdot \sin(\varphi)} \right) \right] \tag{9}$$

The total loss factor necessary in equations (3) and (4) is then:

$$F = F_{tip} \cdot F_{hub} \tag{10}$$

Once the induction factors are determined, the angle of attack is calculated and, by help of the drag and lift coefficient of the section, it leads to the lift and drag forces acting on that section. The local in-plane and out-of-plane forces are then obtained by projection of lift and drag force on the rotor plane and normally to it. By summing the contributions of each section along the blade one can get the total thrust force on this blade and the torque induced by the flow.

This algorithm is employed for both blades and at each time step the blade rotates of an angle $\Delta\gamma$ while the water velocity profile is recalculated at time $t + \Delta t$. The wave-current interaction is very simplified here. The water particle velocity due to waves is only added to the current velocity. However, it generates a new wave frequency, called the frequency of encounter ω_e, expressed as in equation (11). It accounts for the fact the waves travelling in the same direction than the current travel faster and so a fixed body will be subjected to waves of higher frequency as the current velocity increases.

$$\omega_e = \omega_w + k \cdot V \tag{11}$$

The water particle velocity due to waves is expressed in deep water as explained in Faltinsen [9] and the velocity vector can be decomposed into an horizontal component (see equation (12)) and a vertical component (see equation(13)).

$$V_H(x, z, t) = \frac{H_W}{2} . \omega_e . e^{kz} . \sin(\omega_e . t - kx) \tag{12}$$

$$V_V(x, z, t) = \frac{H_W}{2} . \omega_e . e^{kz} . \cos(\omega_e . t - kx) \tag{13}$$

Equations (12) and (13) show that at a given depth each component of the water particle velocity is a sinus function, whose amplitude exponentially decreases with depth. The motion of water particle under wave train is significant down to a depth of half the wave length. It is therefore not possible to totally avoid the region where waves have an effect when installing a tidal turbine.

3.2. Added mass force implementation

The BEM as introduced so far is a quasi-steady approach, which can calculate at each time step the load on a blade section for given constant blade rotational velocity and axial stream velocity, without taking into account the previous time step. Appearance of disturbances in the stream, which can be due to a yaw motion of the rotor, turbulence in the flow, pitching of the blades or ocean waves, induce varying angles of attack in time and dynamic effects if the changes are fast enough.

Several phenomena have been observed on wind turbine blades subjected to dynamic inflow. Among them one can refer to dynamic wake [10] and dynamic stall [11]. They are not taken into account in this study, but will be the subject of further work. Specific to tidal turbine, the high density of water surrounding the turbine blades gives also the possibility for a non-negligible added mass of the blades when rotating in an unsteady stream.

The added mass, m_A , of a body moving in a fluid is an additional force acting on the body, proportional to its acceleration. It is depending on the fluid properties and the body geometry. It is seen as an additional weight due to the fluid particles which have to be moved around the body when this one is accelerating or decelerating through the fluid. Each element of the blade has an added mass which can be approximated by taking the added mass of a cylinder of height dr and diameter the local cord length L_c, as done by Maniaci et al. [5] (equation (14)),

$$m_{A,\ cylinder} = \frac{1}{4} \cdot \pi \cdot {L_c}^2 \cdot \rho \cdot dr \tag{14}$$

The method to derive the added mass force is explained in Maniaci [5] and adapted here for a non-uniform flow field. The kinetic energy, T_A, produced by the added mass phenomenon in the axial direction can be expressed as:

$$T_A = \frac{1}{2} \cdot \rho \cdot \int_V (u - v) \cdot (u - v) \cdot dV \tag{15}$$

where u is the local axial component of fluid velocity and v is the axial component of far field fluid velocity, including waves, at the depth of the considered element.

$$T_A = \frac{1}{2} \cdot \rho \cdot \int_V \frac{(u-v)\cdot(u-v)}{(\bar{u}-v)^2} \cdot dV \cdot (\bar{u} - v)^2 \tag{16}$$

This expression of kinetic energy can also be written as in equation (17), where the added mass is introduced.

$$T_A = \frac{1}{2} \cdot m_A \cdot (\bar{u} - v)^2 \tag{17}$$

where $\bar{u}$ is the mean local flow speed, i.e. corrected by the induction factor and averaged over the blade element.

$$\bar{u} = v \cdot (1 - a) \tag{18}$$

Maniaci looked at a case study where blades are pitching in a constant axial flow, which is not true in a wave field. By using the relation between kinetic energy and work of the added mass force, one can set axial added mass force on a blade element as in equation (19), where, unlike Maniaci's formulation, the time derivative of local water velocity has been introduced to account for changes in water particle velocity.

$$F_A = -\frac{1}{\bar{u}-v} \cdot \frac{dT_A}{dt} = -m_A \cdot \frac{d(\bar{u}-v)}{dt} = -m_A \cdot \frac{d(a\cdot v)}{dt} = -m_A \cdot \left(v \cdot \frac{da}{dt} + a \cdot \frac{dv}{dt}\right) \tag{19}$$

This is of course correct for potential flow only.

Using the same assumptions leads to the derivation of the rotational added mass force on a blade element in non-uniform flow field but with constant rotational speed of the rotor (see equation(20)).

$$F_R = -m_A \cdot \frac{d\left(R \cdot \omega \cdot (1+a')\right)}{dt} = -m_A \cdot R \cdot \omega \cdot \frac{da'}{dt} \qquad (20)$$

These added mass forces F_A and F_R are then respectively added to the axial and tangential elementary forces obtained with the quasi-steady BEM. So the expression of the thrust force on one blade and the shaft torque proposed here are:

$$T_{Added\ mass} = T_{Steady\ BEM} - \frac{1}{4} \cdot \pi \cdot {L_c}^2 \cdot \rho \cdot dr \cdot \left(v \cdot \frac{da}{dt} + a \cdot \frac{dv}{dt}\right) \qquad (21)$$

$$Q_{Added\ mass} = Q_{Steady\ BEM} - \frac{1}{4} \cdot \pi \cdot {L_c}^2 \cdot \rho \cdot dr \cdot R \cdot \omega \cdot \frac{da'}{dt} \cdot r \qquad (22)$$

To account for 3D effects, the commercial code GH Tidal Bladed [12] modifies the classic actuator disc theory by introducing the added mass of a sphere with a radius equal to the turbine radius:

$$m_{A,\ sphere} = \frac{2}{3} \cdot \pi \cdot R^3 \cdot \rho \qquad (23)$$

However, to be compatible with the BEM, the added mass considered for each blade element is assumed to be a spherical shell. The sum of all the shells gives the total added mass of a sphere. This assumption leads to the added mass on one annulus of the actuator disc, of inner radius R_1 and outer radius R_2:

$$m_{A,\ element} = \frac{2}{3} \cdot \pi \cdot \left({R_2}^3 - {R_1}^3\right) \cdot \rho \qquad (24)$$

The steady thrust coefficient for the full annulus of inner radius R_1 and outer radius R_2 is then modified to account for this added mass by using the following differential equation:

$$C_T = 4 \cdot a \cdot (1-a) + \frac{16}{3 \cdot \pi \cdot V} \cdot \frac{{R_2}^3 - {R_1}^3}{{R_2}^2 - {R_1}^2} \cdot \dot{a} \qquad (25)$$

The thrust force considered here is that on one blade and not on the full actuator disc. That is why, for a 2-bladed turbine, the added mass inserted in the thrust force expression is assumed to be half that expressed in equation (24). Finally, the thrust force acting on one blade according to GH Bladed is:

$$T_{GH\ Bladed} = T_{Steady\ BEM} - \frac{1}{3} \cdot \pi \cdot \left(R_2{}^3 - R_1{}^3\right) \cdot \rho \cdot \left(v \cdot \frac{da}{dt}\right) \tag{26}$$

GH Tidal Bladed code does not consider any added force in the tangential direction. The torque resulting of this code is then exactly equal to the one obtained with the quasi-steady BEM.

$$Q_{GH\ Bladed} = Q_{Steady\ BEM} \tag{27}$$

This way of expressing blade elements added mass implies that the load frequency dependency of the added mass is neglected. Wang [13], who looked at the diffraction and radiation of regular waves by a submerged sphere, found out the added mass coefficients in heave and in surge. Given the radius of the reference tidal turbine developed at NTNU, R, and the clearance to the free surface, the added mass in surge and heave of the turbine should be dependent on $k \cdot R$, i.e. on wave characteristics, especially in the region $0.4 \ll k \cdot R \ll 2$. But this is out of the scope of this paper and as Whelan [4] suggested it, the added mass of the turbine is considered constant whatever the wave state.

The full algorithm is summarized on Fig 2, with an optional added mass force which can be calculated as in equations (21) and (22), i.e. the so-called "modified Maniaci method", or as in equations (26) and (27) to use the method employed by GH Tidal Bladed. Note that the commercial software itself was not used.

4. Experiments

A lab-scale model of the reference tidal turbine developed by the Norwegian University of Science and Technology has been tested in a 260m-long towing tank. The 2-bladed horizontal axis rotor has a diameter of 1.475m and is designed for a tip speed ratio of 7 at the design stream velocity of 0.67 m/s. The rotor is installed 1.32m deep under a carriage able to tow the turbine at different constant speeds, while a double flap wave maker generates regular waves at the upstream extremity of the tank. A wave absorber at the other end of the tank avoids any risks of wave reflection on the turbine. The clearance in still water is 0.57m.

The suction sides of the blades have been tripped to ensure the same lift and drag coefficients as in a 20m-diameter full scale despite of a low Reynolds number in the tank. The location of the roughness band was determined using the method explained in [14].

A first efficiency test in still water gave a design efficiency of 43%, which corroborates well with the efficiency estimated by a previous CFD simulation in full scale (42.1%) explained in Faudot et Al [1] and the results given by the BEM in steady flow (42.44%).

Strain gauges located at the root of one blade give the forces (F_x and F_y) and momentums (M_x, M_y and M_z) acting at the root as illustrated on Fig 3. By combining them, torque and thrust force acting on one blade can be calculated.

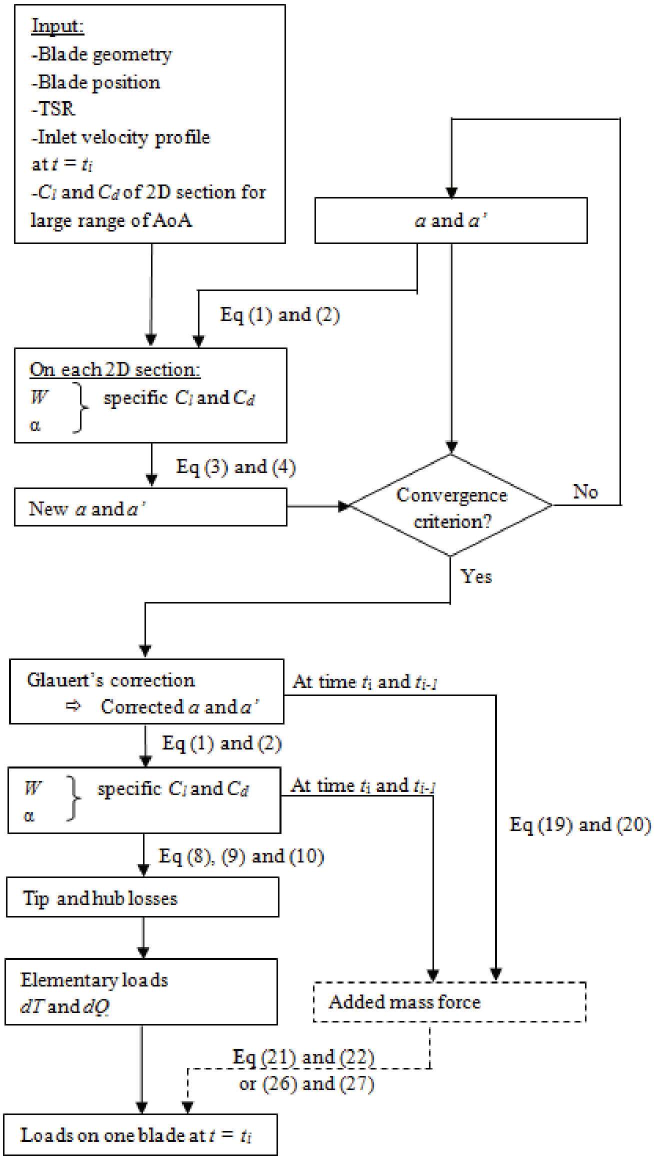

Fig. 2. BEM algorithm in unsteady flow, with optional implementation of added mass force

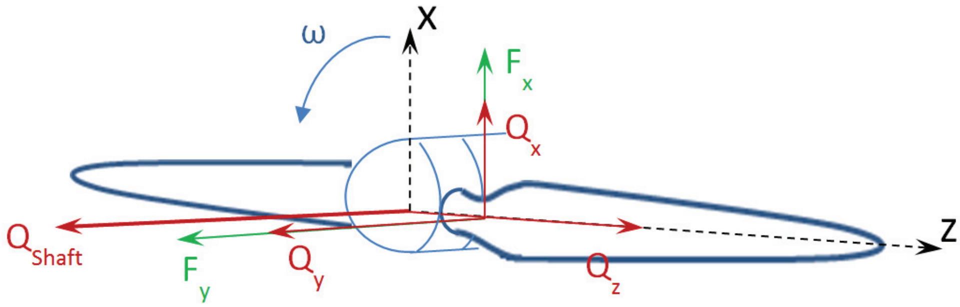

Fig. 3. Rotor and measured quantities

The rotational frequency of the rotor is controlled so that it remains constant even in wave fields. The carriage speed is also constant and not affected by extra loads due to waves.

Water elevation is measured using two types of sensors: resistance and ultrasound wave probes. To assure the quality of waves, wave probes are located near the wave maker, in the plane of the rotor, and few meters upstream (see red dots on Fig 4)

A maximum blockage ratio of 3.5% is calculated. The blockage effects are not supposed to have any influence on the results, but to avoid any deviation, the inflow velocity in the BEM is set to 1.035 times the carriage velocity, as advised in Maskell theory [15] which considers that the flow passing through the turbine is speeded-up and has a velocity of $V \cdot (1+\epsilon)$, where ϵ is the blockage ratio.

A clearance of 4.26m on both sides of the rotor prevents from any wall effects on the rotor. However, a wave train is obviously not as regular after propagating over such a long distance as near the wave maker. That is why wave probes in the surrounding of the rotor are of importance to determine the phase and the real-time amplitude of encountered waves.

5. Results

For this study, several theoretical models have been compared to the experimental results: the steady BEM as explained in the first part of this publication, the steady BEM completed with the added mass implementation used in GH Tidal Bladed commercial software and the steady BEM with a new added mass model, called "modified Maniaci". The mean values and the standard deviations of the loads are reported on different figures. They are representative to the intensity and the amplitude of variations of the loads. It is not a sufficient representation of the loads to carry a complete fatigue analysis of the blades, but gives an insight on the magnitude of the loads compared to the characteristics of waves and current.

The wave states simulated are listed in Table 1.Waves states leading to a current number lower than 1

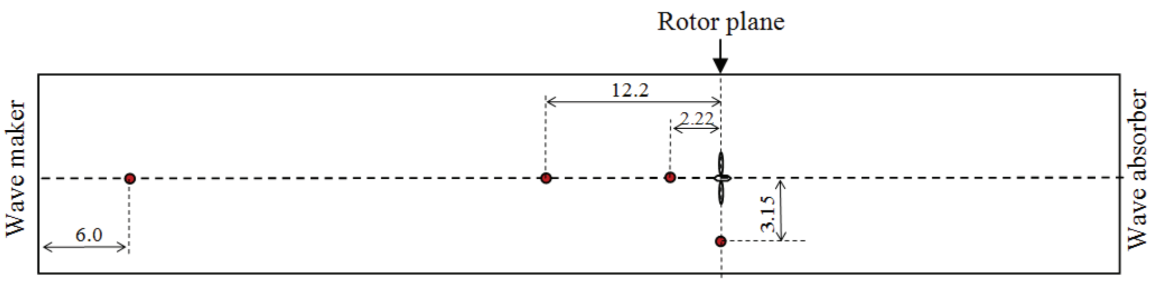

Fig. 4. Towing tank with position of wave probes (red dots)

have been avoided so that water particle velocity at shaft depth remains positive at any time.

Relative current number, μ, at shaft depth is defined as the ratio between current velocity and amplitude of horizontal velocity variations. Since the linear wave theory in infinite deep water is assumed, the horizontal velocity at time t and depth z positive upward is defined as:

$$u(x,z,t) = \frac{H_w}{2}.\omega_w.e^{kz}.\sin(\omega_w.t - kx) \tag{28}$$

where k is the wave number, ω_w the wave frequency, and H_w the wave height.
The amplitude of variation of horizontal water particle velocity is then:

$$u(x,z,t) = \frac{H_w}{2}.\omega_w.e^{kz} \tag{29}$$

This means that the relative current number at shaft depth is expressed as in equation (30):

$$\mu(z_{shaft}) = \frac{V_{current}}{\frac{H_w}{2}.\omega_w.e^{kz_{shaft}}} \tag{30}$$

Table 1. Wave states tested

Current velocity [m/s]	Wave Height [m]	Wave Period [s]	Wave steepness [-]	Relative current number at shaft depth [-]
0.67	0.092	1.332	0.033	61.21
0.27	0.092	1.332	0.033	24.48
1.07	0.092	1.332	0.033	97.94
0.67	0.136	1.332	0.049	41.55
0.27	0.136	1.332	0.049	16.62
1.07	0.136	1.332	0.049	66.48
0.67	0.177	1.883	0.032	10.11
0.27	0.177	1.883	0.032	4.04
1.07	0.177	1.883	0.032	16.18
0.67	0.197	1.332	0.071	28.76
0.27	0.197	1.332	0.071	11.50
1.07	0.197	1.332	0.071	46.02
0.67	0.259	1.883	0.047	6.93
0.27	0.259	1.883	0.047	2.77
1.07	0.259	1.883	0.047	11.09
0.67	0.354	1.883	0.064	5.06
1.07	0.354	1.883	0.064	8.09
0.67	0.371	2.643	0.034	3.24
1.07	0.371	2.643	0.034	5.18
0.67	0.556	2.686	0.049	2.16

1.07	0.556	2.686	0.049	3.43
0.67	0.682	2.686	0.061	1.75

The relative current number gives an idea of the relative importance of wave loads in comparison with current loads. A low relative current number means large variations of particle velocity and thus an angle of attack that can vary from negative values to stall domain. Dynamic effects are then increased at low relative current numbers since the changes of angle of attack are larger and faster.

5.1. Mean loads

Concerning the mean loads, the trends are quite clear: high waves make the mean thrust force and torque drop. This is explained by angles of attack which are very small under a wave through, or even negative. The thrust force is then almost zero. On the contrary, under a wave crest, the horizontal component of water particle velocity due to waves is at its maximum. The angles of attack can thus reach the stall domain, and the torque drops. A combination of both phenomena with the time delay necessary for the flow to reattach in case of stall gives decreased time averaged loads. Once away from the range of relative current number leading to stall or very small angles of attack, mean loads are independent on wave characteristics. Waves leading to relative current number at shaft depth larger than 8 does not have any influence on mean torque, which then is equal to the one measured in still water.

The relative differences between the three methods employed to calculate the loads (steady BEM, steady BEM with the modified Maniaci method to implement added mass force, and steady BEM with GH Tidal Bladed's added mass method) are within 1%. They are then considered as insignificant. It is however interesting to note that these differences are slightly larger for low relative current numbers, i.e. when dynamic effects are of importance.

High and design current speeds are likely to give better accuracy in mean thrust force (mean thrust force within 4% deviation, but within 1.5% for $\mu(z_{shaft}) > 8$) than low speed, which can reach deviation of 8%. Those deviations are the largest at low relative current number because of the low ability of the BEM to deal with stall and the non-implementation of dynamic stall in the present code.

Mean shaft torque is overestimated by the analytical tools, compared to experimental results. But the deviation is within 8% for high and design current speed for $\mu(z_{shaft}) > 5$. At low current speed, were stall is likely to occur more often, the mean shaft torque is overestimated by up to 72%. The deviation at low current speed is due to a Reynolds number much lower than the Reynolds number in the BEM algorithm, which is taken as the design Reynolds number, i.e. at design current velocity and without wave. The lift and drag coefficients are changed with current speed and this has an impact on the total loads, especially at low speed.

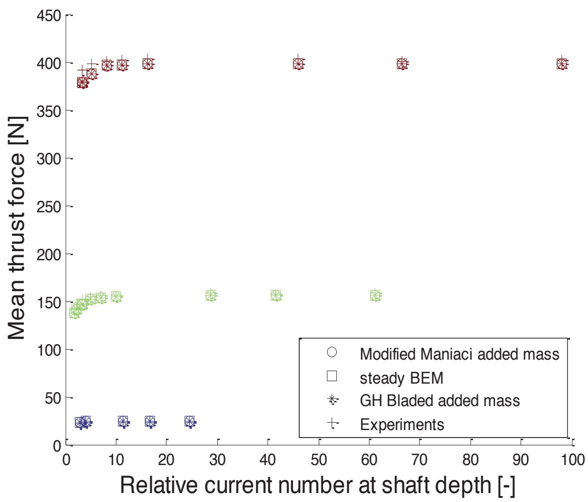

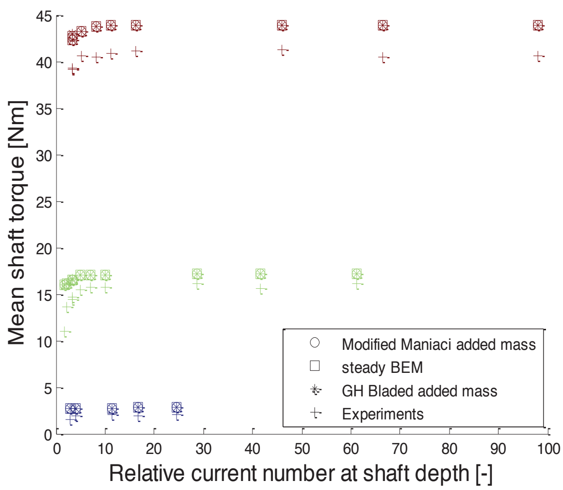

Fig. 5. (a) mean thrust force on one blade. Blue: low current speed (0.27m/s), green: design current speed (0.67m/s), red: high current speed (1.07m/s) ; (b) mean shaft torque

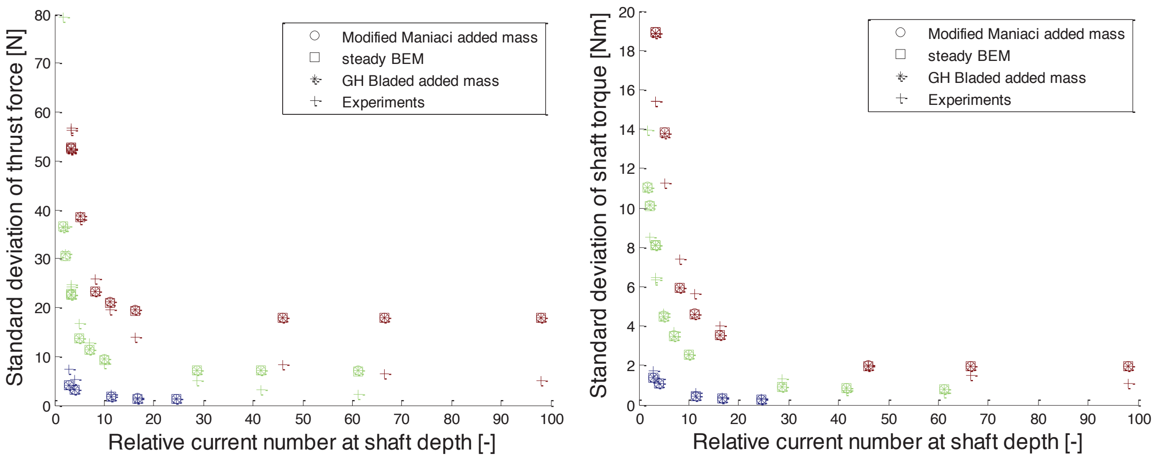

Fig. 6. (a) standard deviation of thrust force on one blade ; (b) standard deviation of shaft torque

5.2. Loads variations

As illustrated in Fig 6, the amplitude of the loads are much increased for low relative current numbers, in experimental results as in all the theoretical results showed here. The theoretical results are so close to each other that it is not easy on Fig 6 to distinguish them. This shows that the added mass of a stiff blade, when wave diffraction is neglected, does not have a significant effect on the loads. This might be wrong for an elastic blade, whose acceleration in all directions is not always zero, or for a pitching blade. Nevertheless, one can see that for higher waves, i.e. low relative current numbers, all theoretical methods do underestimate the thrust force variations, while those are overestimated for small waves. Higher current speed leads to larger deviations in estimation of loads variations, while at design and low current velocities, the theoretical results are very satisfactory, especially for relative current number between 4 and 25. No reason has been found to explain the overestimation of the thrust force variations at high

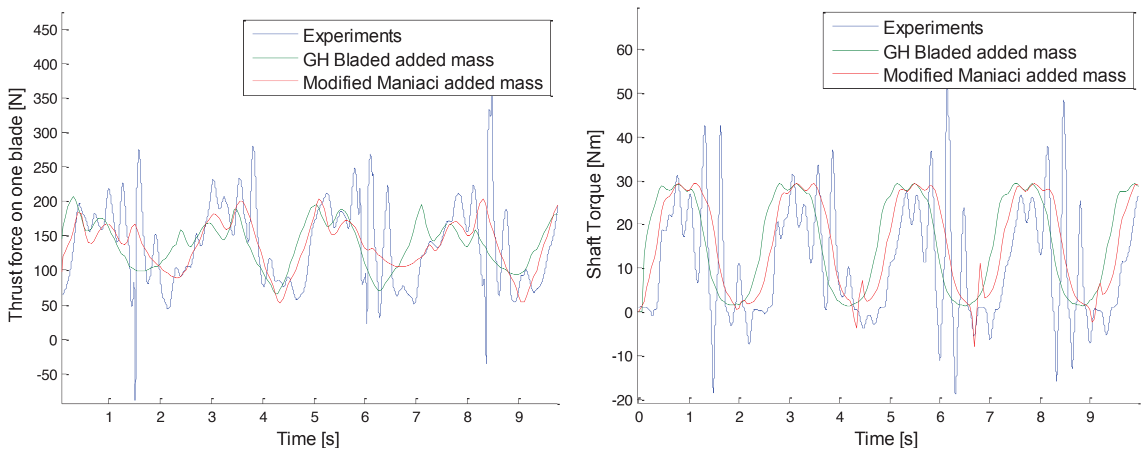

Fig.7. (a) time series of thrust force on one blade for design current speed, H_w=0.682m, T_w=2.686s ; (b) time series of shaft torque for design current speed, H_w=0.682m, T_w=2.686s

relative current numbers. This corresponds to very small waves and even the steady BEM over predicts the amplitude of the signals. This does not mean that higher load peaks are theoretically expected, as shown in Fig 9. The maximum loads are indeed not higher in theory than during the experiments.

The time series of thrust force on one blade (see Fig 7) show the proximity between both theoretical methods, but with a small phase shift, the curve taking into account the time derivative of the local velocity (modified Maniaci method) agreeing better with experimental results. The same remark can be done for the shaft torque.

The reason why experimental results have many additional oscillations after the main peaks is the intensity of those loads. The rotational speed of the blades is maintained constant thanks to a servomotor located on the carriage, and linked to the hub via a long vertical shaft, a mitre-gear and a short horizontal shaft. The sensor measuring the rotational velocity of the turbine (see Fig 8) shows that this speed is not as constant as expected, due to a certain elasticity of the long shaft. It is noticeable that the peaks in thrust force correspond to large rotational accelerations happening after a wave crest passed the swept area. The standard deviation of the rotational speed is less than 0.2 rps in the worst case tested, shown on Fig 7. The experimental results are then considered as acceptable in the region were oscillations amplitudes are smaller. In the theoretical models, the rotational speed of the blades is considered as constant and cannot give such oscillations of loads. That is why we have an underestimation of the standard deviation of loads at low relative current number.

In addition, irregularities in experimental results can also be related to higher harmonic excitation of the blades. Those frequencies can meet the natural frequency of the blade, which enters into resonance. That reveals the need of an hydroelastic implementation of the blade to account for blade structural properties. The deflection can then be calculated at each time step, which will slightly modify the angle of attacks and hydrodynamic coefficients. This kind of information is of importance in the design phase of a blade, to prevent from negative torque, as it happens in the experiments and to carry on a relevant fatigue analysis.

5.3. Extreme loads

Extreme loads are plotted in Fig 9, and both maximum thrust force and torque are well predicted compared to experiments, with a deviation maximum thrust of less than 9% for $\mu(z_{shaft}) > 5$ and a deviation maximum shaft torque of less than 5.3% for $\mu(z_{shaft}) > 5$ at design and high current speed. The deviation is however larger for small current numbers and in the worst case (as illustrated in Fig 7) the varying rotational speed of the turbine during the tests leads to high peaks which should not exist if the rotational speed was kept constant.

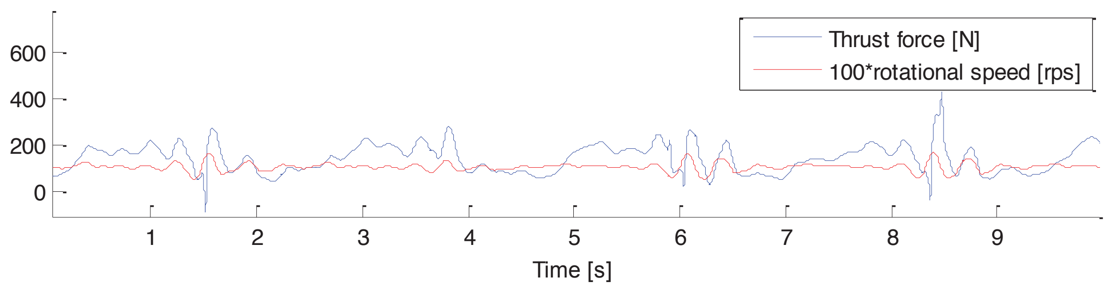

Fig. 8. time series of rotational speed of the blade and thrust force on one blade for design current speed, H_w=0.682m, T_w=2.686s

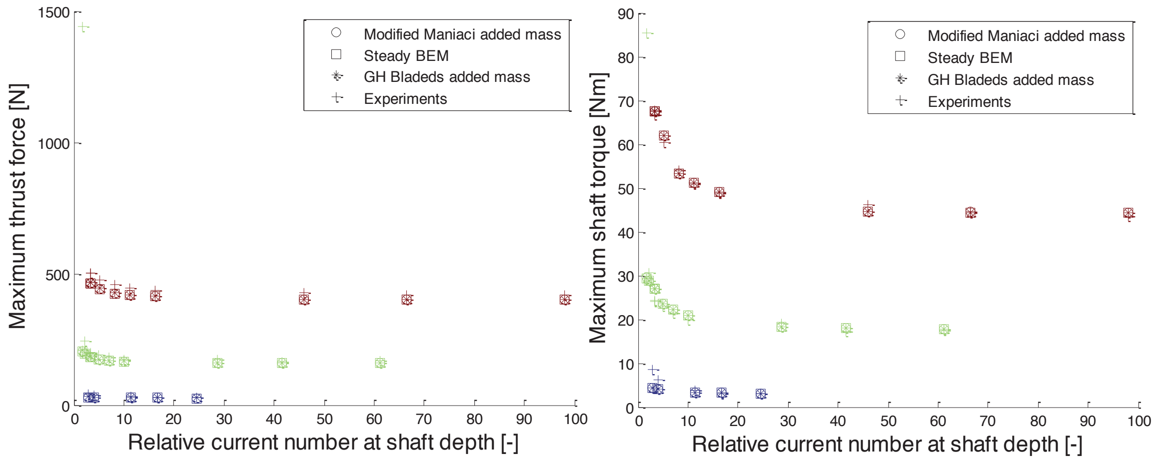

Fig. 9. (a) maximum thrust force on one blade ; (b) maximum shaft torque

6. Discussion of the results and further work

A comparison between two ways of inserting the added mass into a Blade Element Momentum theory algorithm has been done. The quality of both models was then evaluated relative to experimental data. Theoretical and experimental results can be discussed.

Many assumptions have been done to estimate the blade loads in an efficient way. The main one is the assumption that the lift and drag coefficients are independent on the flow and taken as those obtained with X-foil for the design operating conditions. This explains the better agreement between experiments and theory at design speed than lower speed.

In addition, the BEM used here does not take into account dynamic stall or dynamic wake, which leads to larger differences in mean values between theory and experiments for small relative current numbers (i.e. higher and steeper waves). The dynamic effects are of importance in a theoretical model which would have for objective an exact determination of extreme and fatigue loads.

The blades are considered as infinitely stiff, which is of course not the case when loads are large. A hydroelastic model would show the deflection of the blade and modify the angle of attack, especially in higher current speed. Moreover, higher order waves can excite the blade at their natural frequency, generating vibration, which, combined with a dynamical model, leads to a more accurate prediction of the loads. Vibrations of the blades lead to higher time derivatives of induction factors and local relative velocity. This would have an effect on the added mass forces.

Concerning the experiments, which were used in the publication as the reference, it has been shown that the rotational speed of the blades was not as constant as planned. To fit with experimental data, the varying rotational speed should be an input parameter in theoretical models. Moreover, the deflection of the blades was visible but not measured during the tests.

The deviations between theoretical and experimental results cannot only be explained by the assumption of stiff blade, but are also due to other dynamic effects. The next step in this estimation of blade loads in non-uniform flow is therefore to find and implement a robust dynamic wake and dynamic stall model, which could be compatible with Blade Element Momentum theory applied on each blade separately.

The diffraction of waves by the turbine and the load frequency dependency of the added mass will also be investigated in a further study. Knowing the real behavior of the flow around the turbine will give a better understanding of blade loads in a wave field.

The insignificant difference between theoretical loads with or without added mass force fits with Whelan's conclusion [4] because of the stiff blade assumption, the constant rotational speed and the absence of pitching. In a more realistic case study, added mass would have, as suggested by Maniaci [5], an effect on blade loads.

7. Conclusion

This paper shows in which kind of sea state the steady blade element momentum theory can be relevant, and for what kind of waves an additional implementation of dynamic effects is necessary. The BEM is revealed to be accurate in a larger frame than expected both in terms of mean loads and load variations. The steady BEM applied on a stiff blade is indeed satisfactory for relative current number at shaft depth larger than 8.

However extreme loads, essentially due to high and steep waves, are of importance for the design of any blade and this method is not sufficient for low relative current number. Additional dynamic effects like dynamic stall and dynamic wake are then necessary to estimate the loads in very steep waves.

The implementation of added mass in a non-uniform inflow has not shown any important effect on the loads. But this added mass implementation can get significant with non-stiff blades, if combined with hydroelastic model of the blades.

Acknowledgements

This research was carried out as part of the Statkraft Ocean Energy Research Program, sponsored by Statkraft (www.statkraft.no). This support is gratefully acknowledged.

References

[1] Faudot C., Dahlhaug O.G., Tidal turbine blades: design and dynamic loads estimation using CFD and blade element momentum theory. *Proceedings of the 30th International Conference on Ocean Offshore and Arctic Engineering*, Rotterdam, Netherland; 2011.

[2] Masters, I., Chapman, J.C., Willis, M.R., Orme, J.A.C. A robust Blade Element Momentum Theory model for tidal stream turbines including tip and hub loss corrections. *Proceedings of the Institute of Marine Engineering, Science and Technology Part A: Journal of Marine Engineering and Technology*, 10 (1); 2011, pp. 25-35.

[3] Baltrop N, Varyani K.S., Grant A., Clelland D., Pham X.P., Investigation into Wave-Current Interactions in Marine Current Turbines IMechE Vol 221 Part A; 2007.

[4] Whelan J. I., Graham J. M. R., Peir´o J., Inertia Effects on Horizontal Axis Tidal-Stream Turbines, *Proceedings of the 8th European Wave and Tidal Energy Conference*, Uppsala, Sweden; 2009.

[5] Maniaci, D.C., Ye Li, Investigating the influence of the added mass effect to marine hydrokinetic horizontal-axis turbines using a General Dynamic Wake wind turbine code, *OCEANS 2011*, 19-22; 2011, pp.1-6.

[6] Hansen M.O.L, *Aerodynamics of Wind Turbines (2nd Edition)*, Earthscan, ISBN: 978-1-84407-438-9;2008, pp. 45-55.

[7] Batten W.M.J., Bahaj A.S., Molland A.F., Chaplin J.R., Prediction of the Hydrodynamic Performance of Marine Current Turbines, Renewable Energy; 2008; 33:1085-1096.

[8] Drela M., XFOIL 6.5 User Primer; 1995.

[9] Faltinsen O.M., *Sea Loads on Ships and Offshore Structures*. Cambridge University Press; 1990.

[10] Hansen M.O.L, *Aerodynamics of Wind Turbines (2nd Edition)*, Earthscan, ISBN: 978-1-84407-438-9; 2008, pp. 93-95

[11] Hansen MH, Gaunaa M, Madsen HAa. A Beddoes-Leishman type dynamic stall model in state-space and indicial formulations. Technical Report Risø–R–1354(EN), Risø National Laboratory; 2004.

[12] E. A. Bossanyi, GH Tidal Bladed Theory Manual, Garrad Hassan and Partners Limited; 2008, pp. 9-10.

[13] Wang, S. Motions of a spherical submarine in waves. *Ocean Engineering*, 13 (3); 1986, p. 249-271.

[14] Braslow A.L., Knox E. C., Simplified method for determination of critical height of distributed roughness particles for boundary-layer transition at Mach from 0 to 5, NACA Technical Note 4363; 1958.

[15] Whelan J. I., Graham J. M. R., Peir´o J., A free surface and blockage correction for tidal turbines. J*ournal of Fluid Mechanics*, 624:281–291; 2009.